Analysis of Geometric Accuracy in Digital Breast Tomosynthesis Reconstruction

Predrag R. Bakic[1], Peter Ringer[2], Johnny Kuo[2], Susan Ng[2], and Andrew D.A. Maidment[1]

[1] University of Pennsylvania, Dept. of Radiology, Philadelphia, PA 19104
[2] Real-Time Tomography, LLC, Villanova, PA19085
{Predrag.Bakic,Andrew.Maidment}@uphs.upenn.edu,
{Peter.Ringer,Johnny.Kuo,Susan.Ng}@realtimetomography.com

Abstract. The geometric accuracy of a digital breast tomosynthesis (DBT) reconstruction algorithm was assessed using an anthropomorphic software breast phantom with simulated fiducial markers. The locations of the fiducial markers were measured from supersampled images reconstructed to sub-pixel precision. The measured locations were compared with the known ground truth positions of the simulated markers. The fiducial markers simulate small, attenuating objects within the software phantom. Using reconstructed images with resolution of 0.115 mm, and a total of twelve fiducial markers at three different depths, we determined an average difference of 0.105 mm (st. dev. 0.086 mm) between the estimated and true marker locations.

Keywords: Anthropomorphic breast phantom, tomosynthesis, tomographic reconstruction algorithms, geometric accuracy of tomographic reconstruction.

1 Introduction

DBT is an investigational imaging modality that offers improved visualization of breast tissue by eliminating tissue overlap. Early clinical studies have shown that DBT has increased sensitivity and specificity compared to digital mammography (DM), the current gold standard in breast cancer screening. With a radiation dose comparable to DM, DBT has the potential to replace DM as the standard breast cancer screening modality.

Methods for analyzing DBT systems using physical test objects have been described in the literature; these methods use physical test objects, such as a slanted wire [1], or custom-made calibration phantoms [2]. Currently, however, no generally accepted standards exist for testing DBT acquisition and reconstruction. The three-dimensional nature of DBT limits the use of existing tools for mammography (*e.g.*, mammographic accreditation phantom [3]). Similarly, the limited angular range of DBT acquisition prevents the use of most clinical CT tools. In this paper, we describe preliminary results of estimating the geometric accuracy of a DBT reconstruction algorithm using an anthropomorphic software breast phantom with fiducial markers simulated at known positions.

J. Martí et al. (Eds.): IWDM 2010, LNCS 6136, pp. 62–69, 2010.

2 Materials and Methods

We used an anthropomorphic breast phantom described previously [4,5]. The phantom simulates both a realistic breast outline typical of the geometric extent of the breast, and internal tissue structures (glandular tissue, adipose compartments and Cooper's ligaments). The design of the phantom is flexible, covering anatomical variations in breast composition and size. The phantom deformation during clinical breast compression is simulated using a finite element tissue model.

In this study, the breast phantom was simulated with an isotropic resolution of 200 microns. The phantom volume was 450 ml with a compressed thickness of 5 cm and an overall glandularity of 40%. The fiducial markers simulated small, attenuating objects with a size of one voxel (200 microns) and a linear x-ray attenuation 30 times larger than the attenuation of fibroglandular breast tissue. Four fiducial markers were simulated at three different distances from the breast support (6.4 mm, 25.6 mm and 44.8 mm). At each depth, the four markers were positioned in a 20 mm square. Fig. 1 illustrates simulated fiducial markers at different distances from the breast support.

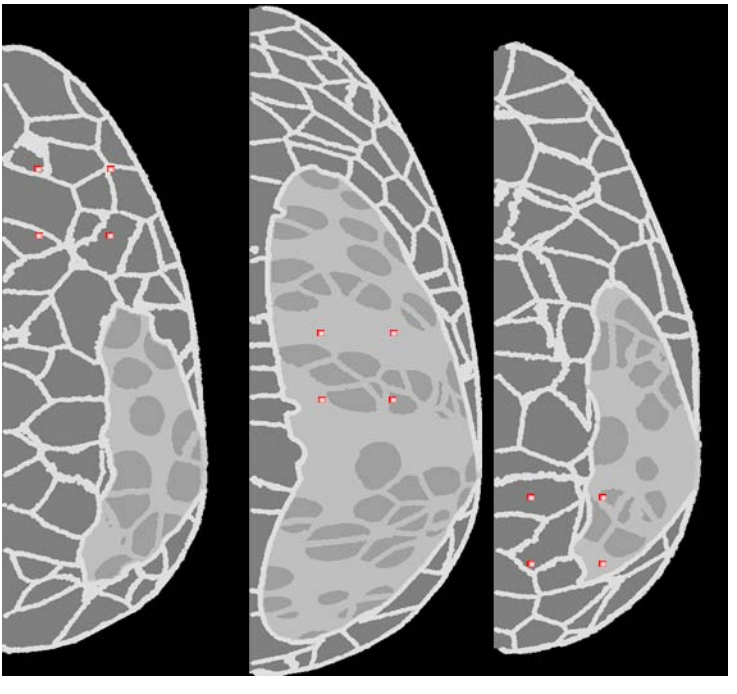

Fig. 1. Cross-sections of the software breast phantom at 6.4 mm (left), 25.6 mm (center), and 44.8 mm (right) from the breast support, containing fiducial markers (in red/white). The markers are shown as magnified 20-fold relative to their simulated size.

Tomosynthesis image acquisition was simulated assuming a monoenergetic x-ray beam without scatter and an ideal x-ray detector. Ray tracing was used to calculate the x-ray attenuation through the phantom. The resolution of the projection images was 100 microns, consistent with the GE Senographe DS tomosynthesis prototype (GE Healthcare, Chalfont St. Giles, UK). The simulated acquisition geometry included 15 projection acquired over a 40 degree arc corresponding to the acquisition protocol of the GE prototype. A commercial back-projection filtered DBT reconstruction algorithm developed by Real Time Tomography, LLC (Villanova, PA) was used. Fig. 2 shows details of a simulated DBT phantom projection (acquired perpendicular to the detector plane) and the reconstructed image plane corresponding to a depth 25.6 mm measured from the breast support.

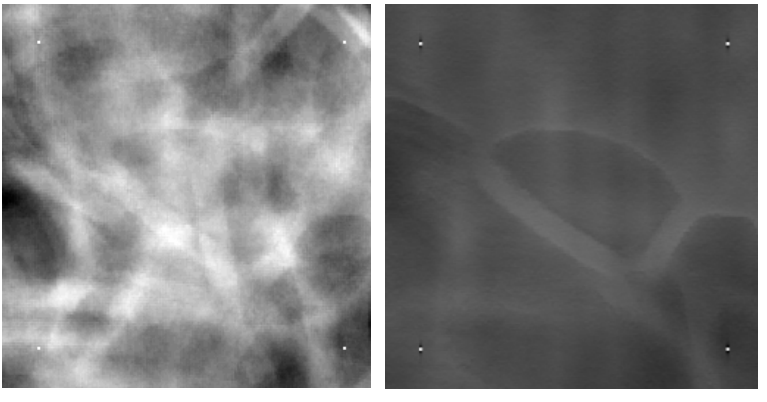

Fig. 2. A detail of a simulated DBT projection image (left) and the reconstructed image plane corresponding to a depth 25.6 mm from the breast support (right) showing four fiducial markers

The reconstruction algorithm used allows us to specify the geometry of the reconstruction plane with arbitrary precision. To measure geometric accuracy, we reconstructed a series of images with sub-pixel shifts within the plane of reconstruction. These images were combined to form a supersampled image. In the current work, 10-fold supersampling was performed in the y-axis (scanning direction) only. In future work, supersampling in the x- and y-axes will be performed. Fig. 3 shows a surface plot of a supersampled image of a fiducial marker.

For our analysis, images of the software phantom with the fiducial markers were reconstructed at a spatial resolution of 0.115 mm, selected to allow display of a 230.4 mm × 192.0 mm reconstructed field-of-view on a 2048×1536 monitor. Image planes were reconstructed every 0.2 mm. For each of the 12 fiducial markers, we identified the distance z_C from the breast support to the reconstructed image plane in which the spatial extent of the objects was smallest. In this plane, we calculated the centroid, i.e., the center of mass, (x_C, y_C) of the marker to determine its location more precisely. The centroid was calculated in a thresholded image of the supersampled objects. The threshold was selected as half of the maximum reconstructed voxel intensity in the region of interest of the fiducial marker.

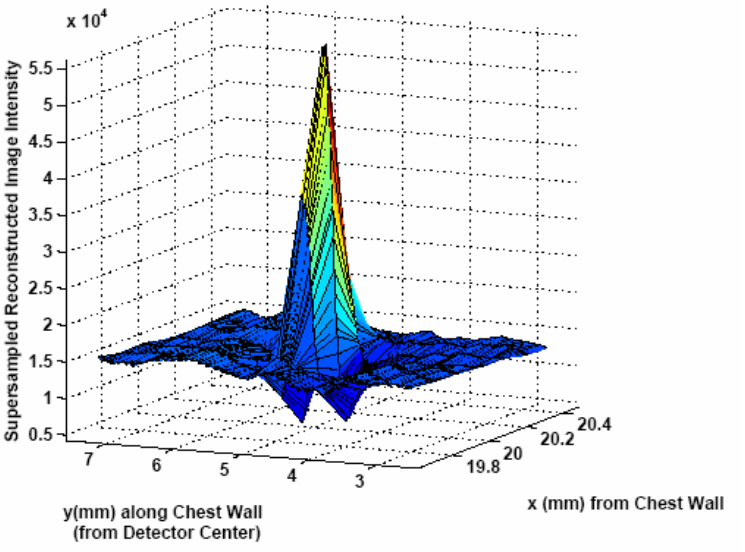

Fig. 3. A surface plot of a supersampled image of a fiducial marker used for estimating the marker location in the reconstructed space with a subpixel precision

The coordinates (x_C, y_C, z_C) were considered as the position of the marker in the three-dimensional reconstructed image space. This position was compared with the known ground truth marker location in the phantom (x_T, y_T, z_T). We defined the error in the position of the fiducial markers E_P as the Euclidean distance between the measured and the true marker position:

$$E_P = \sqrt{(x_C - x_T)^2 + (y_C - y_T)^2 + (z_C - z_T)^2} \quad . \tag{1}$$

In addition, we also calculated the error in the distance between a pair of reconstructed fiducial markers, defined as $E_D = d_R - d_T$, where

$$d_R = \sqrt{(x_{C1} - x_{C2})^2 + (y_{C1} - y_{C2})^2 + (z_{C1} - z_{C2})^2} \tag{2}$$

and

$$d_T = \sqrt{(x_{T1} - x_{T2})^2 + (y_{T1} - y_{T2})^2 + (z_{T1} - z_{T2})^2} \quad . \tag{3}$$

and indices *C1* and *C2* denote the measured and *T1* and *T2* the true locations for a pair of markers.

Using the supersampled images, we also calculated the relative error in estimating marker size from images reconstructed at a given distance from the plane in which the object is in focus. The estimated marker size was calculated as the full width at half

maximum (FWHM) of the reconstructed marker profile. The relative error in marker size was defined as $100\% \times [F(z) - F_{min}]/F_{min}$, where $F(z)$ and F_{min} represent the FWHM estimated at the reconstructed depth z, and the minimum FWHM estimated at the plane of focus, respectively.

3 Results

Fig. 4 shows the error in the measured marker positions E_P as a function of the reconstructed plane depth (*i.e.*, the distance from the breast support). Also shown are the errors calculated separately for each of the three marker coordinates: perpendicular to the chest wall $(x_C\text{-}x_T)$, parallel to the chest wall $(y_C\text{-}y_T)$, and perpendicular to the detector $(z_C\text{-}z_T)$. The overall error E_P averaged over all 12 fiducial markers was 0.105±0.086 mm (average ± st.dev). For the markers located 6.4 mm from the breast support the error E_P was 0.126±0.088 mm; for the markers at 25.6 mm, E_P was 0.073±0.085 mm, and for the markers at 44.8 mm, E_P was 0.116±0.101 mm.

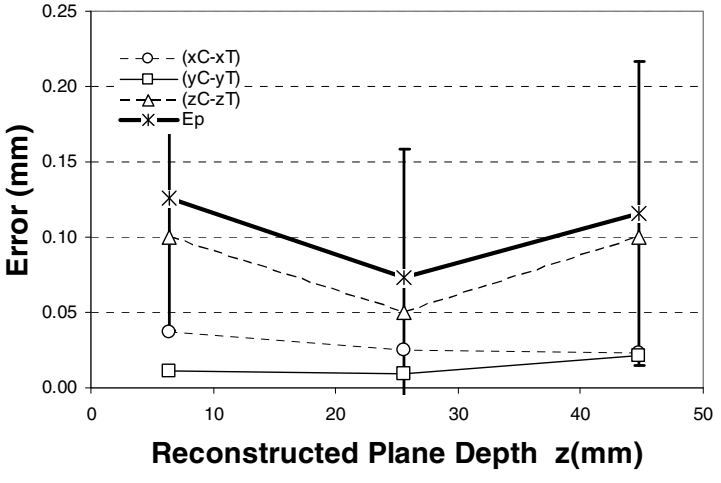

Fig. 4. Average error in the measured 3D position of reconstructed fiducial markers (E_P) as a function of the reconstructed plane depth. (Error bars represent one standard deviation.) Shown also are the errors calculated separately for each marker coordinate.

Fig. 5 shows the error in the reconstructed distance between pairs of fiducial markers E_D. The simulated distance between the markers in the phantom was 20 mm. The distance error is calculated separately for distances measured along the x- and y-axes. The total error E_D averaged over 12 pairs of markers along the two axes was 0.017±0.020 mm. For the markers at a 6.4 mm from the breast support the error E_D was 0.013±0.009 mm; at 25.6 mm, E_D was 0.009±0.007 mm, and at 44.8 mm, E_D was 0.029±0.021 mm.

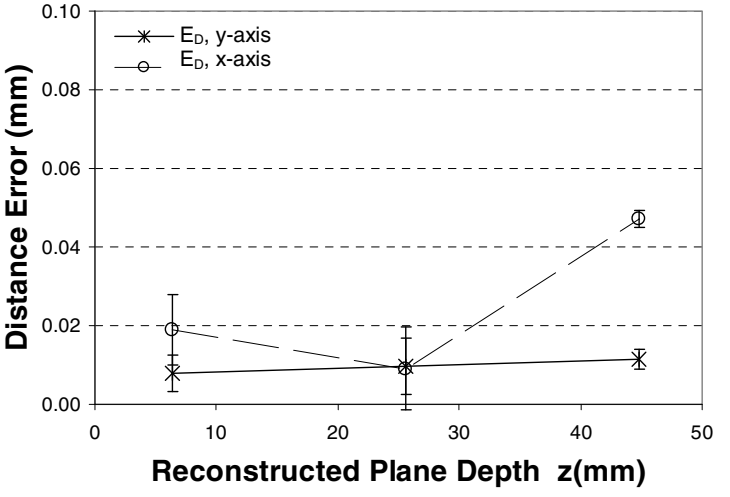

Fig. 5. Error in the reconstructed distance between pairs of fiducial markers (E_D) plotted as a function of the reconstructed plane depth. E_D values were averaged separately over distance measured along the y-axis parallel with tube motion (*) and the x-axis perpendicular to tube motion (○). Error bars represent one standard deviation. Note that supersampling was performed along the y-axis only.

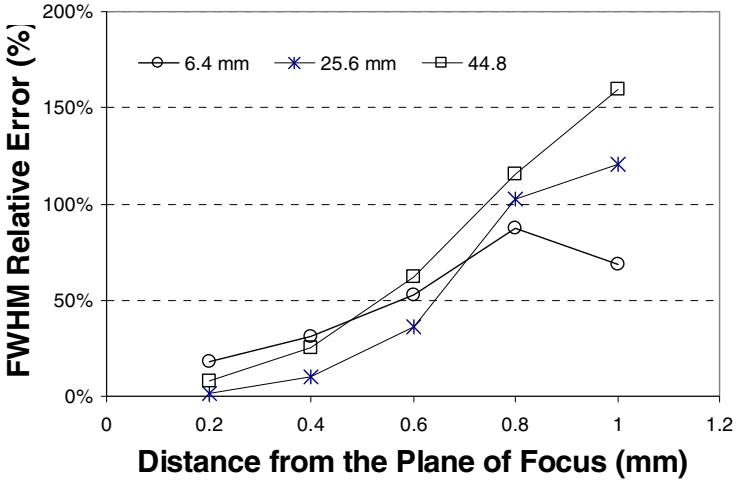

Fig. 6. Relative error in the estimation of the object size at a given distance from the plane of focus, averaged over the fiducial markers positioned at different reconstructed plane depths

Fig. 6 shows the relative error in estimating marker size from images reconstructed at a given distance from the plane of focus. Plotted are the relative errors averaged over the four markers positioned at the same depth. Averaged over all 12 markers, the relative error in estimating marker size at a distance of 0.6 mm away from the plane of focus is equal to 50%; while at a distance of 1.0 mm, the relative error is 116%. The error increases with distance from the detector.

4 Discussion and Conclusions

We have developed a method to assess geometric accuracy with sub-pixel precision. In the example presented, we observed very little dependence of the geometric accuracy on the reconstructed plane; the errors in the measured marker positions E_P were comparable at different distances from the detector. As shown in Fig. 4, the E_P values are on the order of the size of 1 pixel. This is as expected for a well-designed reconstruction system. Note that the error in the z-axis is worst; this arises from the limited angular range of the DBT acquisition geometry.

The observed error in measuring the distance between pairs of fiducial markers E_D, shown in Fig. 5, was a fraction of the pixel size. The E_D values were smaller for distances measured along the y-axis than the x-axis because we performed supersampling along the y-axis only. We plan to extend the presented approach to the analysis of images supersampled in both in-plane directions. The error in distance measurement does not show a strong dependence on the reconstruction plane.

These results have importance for developers of DBT-guided biopsy systems. Based on these data, biopsy systems should be able to localize objects to within one voxel in 3-dimensions, thus providing targeting accuracy comparable to stereotactic biopsy systems.

The presented approach also allowed us to estimate the unsharpness of each object when reconstructed at a given depth from the plane of focus. As shown in Fig. 6, the FWHM error at a distance of 1.0 mm is about twice as large (116% vs. 50%) as at a distance of 0.6 mm. This result is of practical importance as it elucidates limitations of DBT reconstruction in visualizing objects located at a position between two planes of reconstruction. As the analyzed fiducial objects were of size 1-voxel in the phantom, the reconstructed supersampled images of these objects could also be used to calculate spatial dependence of the point spread function.

We are currently performing verification of the presented assessment methodology by analyzing images reconstructed at different magnification. Fig. 7 shows a fiducial marker supersampled 10-times in the y-axis (scan direction), and the same marker from an image reconstructed at 10-times magnification. The images are substantially equivalent; however, accurate side-by-side comparison will require supersampling in both the x- and y-axes, and application of reconstruction filters that are matched in the two magnifications.

In order to validate the effects of simulated image acquisition of the observer accuracy, we also plan to extend the presented approach to include the analysis of physical phantom images. The combined analysis of simulated and physical phantom images offers more flexibility in assessing the impact of the acquisition geometry and system components (e.g., focal spot blurring, scatter, step-and-shoot vs. continuous tube motion, etc.).

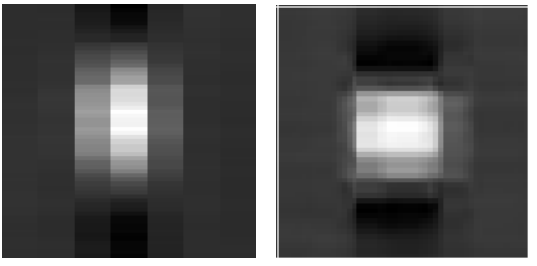

(a) (b)

Fig. 7. The same fiducial marker shown in (a) an image supersampled in the (vertical) direction along the chest wall and (b) a 10 times magnified image

In summary, while physical phantoms can exactly measure individual imaging systems, software phantoms offer an advantage of repeated and potentially automated analysis of a large number of acquisition and reconstruction parameter combinations. Moreover, software breast phantoms include simulated anatomical noise. This is particularly relevant in DBT systems, where the reconstruction algorithm must successfully blur out-of-plane objects while preserving in-plane features.

Acknowledgments. This work in progress has been supported by a subcontract from grant R44EB07140 (Real Time Tomography, LLC.) from the National Institutes of Health. P. Ringer, J. Kuo, and S. Ng are employees, and A. Maidment is chair of the Scientific Advisory Board of Real Time Tomography, LLC. The contents of this paper are solely the responsibility of the authors and do not necessarily represent the official views of the funding agencies.

References

1. Hu, Y.-H., Zhao, B., Zhao., W.: Image artifacts in digital breast tomosynthesis: Investigation of the effects of system geometry and reconstruction parameters using a linear system approach. Medica Physics 35, 5242–5252 (2008)
2. Wang, X., Mainprize, J.G., Kempstone, M.P., Mawdsley, G.E., Yaffe, M.J.: Digital Breast Tomosynthesis Geometry Calibration. In: SPIE Medical Imaging 2007: Physics in Medical Imaging (2007)
3. CIRS Tissue Simulation and Phantom Technology: Mammographic Accreditation Phantom, `http://www.cirsinc.com/015_mammo.html` (accessed on January 17, 2009)
4. Bakic, P.R., Albert, M., Brzakovic, D., Maidment, A.D.A.: Mammogram synthesis using a 3D simulation. I. Breast tissue model and image acquisition simulation. Medical Physics 29, 2131–2139 (2002)
5. Zhang, C., Bakic, P.R., Maidment, A.D.A.: Development of an Anthropomorphic Breast Software Phantom Based on Region Growing Algorithm. In: Visualization, Image-guided procedures, and Modeling, Proc. SPIE, vol. 6918 (2008)